Int. J. Electrochem. Sci., 12 **(2017)** 4406 – 4416, doi: 10.20964/2017.05.79

International Journal of
ELECTROCHEMICAL
SCIENCE
www.electrochemsci.org

Electrochemical Determination of Ganopsoreric Acid A in Ganoderma

Lejun Gao[1,*], *Shuhua Wang*[2], *Xiao Gao*[3]

[1] Department of blood transfusion, Affiliated Hospital of Binzhou Medical College, Binzhou，256610, P. R. China
[2] The discharged patients revisit office, Binzhou City People' s Hospital, Binzhou, 256610, P. R. China
[3] The Department of Pharmacy , Binzhou City People' s Hospital, Binzhou, 256610, P. R. China
[*]E-mail: gaolejun_bz@126.com

Received: 3 February 2017 / *Accepted:* 12 March 2017 / *Published:* 12 April 2017

A simple and effective electrochemical sensor with an electrode modified with an RGO/Au (reduced graphene oxide-gold nanoparticles) nanocomposite was developed for the determination of ganopsoreric acid A, an effective anti-ovarian tumor component. A microwave-assisted approach was adopted to prepare RGO, and RGO/Au was obtained by electrodepositing Au nanoparticles on RGO. Subsequently, the analysis of the electrochemical performance of the developed sensor regarding the reduction of ganopsoreric acid A was accomplished through electrochemical impedance spectroscopy (EIS) and cyclic voltammetry (CV). The electrochemical activity of ganopsoreric acid A reduction was significantly enhanced using the RGO/Au nanocomposite-modified electrode. On this sensor, the linear reaction range was found to be 2 μM to 600 μM. Moreover, the application range of the developed sensor was very wide and was applied for the detection of ganopsoreric acid A in ganoderma herb. The proposed electrochemical determination method could be used for the application of clinical anti-ovarian tumor drug detection.

Keywords: Electrochemistry; Ovarian tumor; Ganoderma; Nanocomposite; Ganopsoreric acid A

1. INTRODUCTION

Ovarian cancer refers to a type of cancer that develops inside an ovary. It can lead to the formation of abnormal cells, which possess the capacity to intrude or diffuse to other sections of the body. At the beginning of this process, either no symptoms or only unclear symptoms are observed. With the development of processes to detect ovarian cancer, symptoms become more recognizable. The symptoms of ovarian cancer include bloating, lack of appetite, and pelvic pain [1, 2]. The

diffusion of this cancer is most likely to occur in the lining of the stomach, bowel and bladder, lungs, lymph nodes, and liver. For women that have ovulated more throughout their life, the possibility for them to have ovarian cancer is higher [3-5]. This is inclusive of those who have never had kids, those who start ovulation when they are young and those who reach menopause when they are old. There are several other risk factors, such as fertility medication, obesity and hormone therapy. Factors such as hormonal contraception, breast feeding and tubal ligation can reduce the risk of ovarian cancer. Approximately 10% of cases are in connection with inherited genetic risk; women whose BRCA1 or BRCA2 gene is mutated have an approximately 50% higher probability of contracting this disease. Ovarian carcinoma, the most common category of ovarian cancer, is related to over 95% of all cases. It mainly has five subcategories, among which the most common one is high-level serous carcinoma [6, 7]. Although parts of these tumors are developed in the Fallopian tubes, it is believed that the development of the tumors first occurs in the cells overlaying the ovaries. In addition, germ cell tumors as well as sexual cord stromal tumors are two kinds of ovarian cancer; however, they are less common. A diagnosis of ovarian cancer is determined by a tissue biopsy, which is always removed in the surgical process.

There is a long history of applying medicinal mushrooms to conventional eastern therapies. Currently, many Asian states, such as China, Japan and Korea, still depend on mushroom-derived preparations to implement clinical practices [8-13]. The medicinal effects of lots of conventionally adopted mushrooms have already been illustrated, which include species extracted from genera Auricularia, Pleurotus, Trametes (Coriolus), Enoki Mushroom, Lucid Ganoderma, Schizophyllum, Hericium, Grifola, Lentinus (Lentinula) and Tremella.

Mizushina et al. [14] and Tanaka et al. [15] separated novel triterpenoid complexes, designated fomitellic acids A and B, from *Fomitella fraxinea*, a type of basidiomycete, which restrained the activities of mammalian nucleic acid polymerase (DNA P) α and β selectively. In recent years, Mizushina et al. [16] reported that the aforementioned triterpenoids were effective depressors of calf DNA polymerase α, mouse DNA polymerase β, and human DNA topo I and II and revealed the moderate inhibitory action on plant DNA polymerase II as well as human immunodeficiency virus transcriptase inverse (HIV). Nevertheless, the complexes had no impact on the activities of DNA polymerases of prokaryotes, such as *E. coli* DNA polymerase I, and other DNA metabolic enzymes, such as human telomerase, T7 RNA polymerase, or bovine deoxyribonuclease I. These triterpenoids were depressors of both mammalian DNA polymerase and DNA topo I and II despite the enzymatic characteristics of DNA polymerases and DNA topos being different from each other to a great extent, including differences in covering their action pattern, three-dimensional construction, and amino acid sequences. There was no binding between these triterpenoids and DNA, indicating that they play a direct role on these enzymes. Fomitellic acid A hindered the development of NUGC gastric cancer cells with LD_{50} values of 38 μM or 30 μM [16]. Terpenoids 1, 2 and 3 that selectively obstruct eukaryotic DNA polymerase movements were segregated from the sporocarp of the basidiomycete *Ganoderma lucidum*, and spectroscopic analysis determined their structures. Novel terpenes, lucidenic acid O and lucidenic lactone, prevented the actions of calf DNA polymerase α, rat DNA polymerase β, and HIV type 1 transcriptase inverse. Cerevisterol, a third novel terpene that was demonstrated as a cytotoxic steroid, merely delayed the activity of DNA polymerase α [17].

Electrochemistry, a widely used effective analytical technique, possesses a variety of merits, such as outstanding sensitivity and reproducibility, high accuracy and precision, a wide linear dynamic scope, and the ability to use cost-effective instruments [18-21]. In medical research, many problems related to medicines can be effectively solved through electroanalytical approaches. Lately, many approaches, such as the development of pulse methods with higher sensitivity, have been commonly applied to component investigations of drugs in the form of dosage or special biological specimens. Carbon-based electrochemical sensors, characterized by their excellent biocompatibility, cost effectiveness, high chemical stability, and outstanding electron-transfer kinetics, have been applied to many fields. In general, the conventional electrodes in sensors are based on carbon in the form of carbon fibers, pyrolytic graphite and glassy carbon. In recent years, novel carbon nanomaterials have shown to have a high potential to be employed in the aforementioned sensors with excellent performance. Generally, the size of the nanomaterials range from 1 to 100 nm. This is due to the high specific surface area as well as high surface-to-volume ratio at these sizes. As a result, carbon nanomaterials are superior to many conventional electrode materials on account of their improved electrocatalytic activity due to quicker electron-transfer kinetics and better interfacial absorption attributes [22, 23].

In this report, the determination of triterpenoid was realized for the first time with the adoption of a simple and precise electrochemical sensor with a graphene-Au nanocomposite-modified electrode. The development of this electrochemical sensor has the capacity to assess the quantity of triterpenoid in its medical preparations around industry. In addition, the determination of the quantity of triterpenoid inside an herb ganoderma was accomplished as well.

2. EXPERIMENTAL

2.1. Chemicals

Ganopsoreic acid A, $HAuCl_4 \cdot 3H_2O$, synthetic graphite (average particle diameter was smaller than 20 μm) and PDDA (poly(diallyl dimethyl ammonium chloride), 20 wt.%, MW=100000-200000 g/mol) were obtained from Sigma-Aldrich and purified by an additional step. In addition, there were other chemicals that served as reagents for the analysis. The synthesis of the phosphate buffer solution (PBS) was as follows: first, a 0.1 M KH_2PO_4 solution was combined with a 0.1 M K_2HPO_4 solution, and the pH of the developed solution was adjusted. Throughout the experiments, Milli-Q water (18.2 MΩ cm) was used.

2.2. Preparation of the graphene-Au nanocomposite

The synthesis of reduced graphene oxide (RGO) was achieved through a previously developed microwave-heating approach with some changes [24]. To 5 mL of a GO aqueous dispersion (0.5 g mL^{-1}), 5 mL of PDDA solution (1 mg mL^{-1}) was added. After this, the mixed solution was sonicated for a half hour. After, the pH value was adjusted to 12.0, and the mixture underwent heating by microwave

radiation for 5 min to functionalize the surface and reduce the GO. Subsequently, the formed solution was isolated through centrifugation (10000 rpm, 10 min), and acquired, dark colored deposit was washed with water three times. Finally, the RGO (acquired black deposit) was dried in an oven at a temperature of 70°C for half a day. The preparation of the RGO/Au/GCE electrode was performed through the sedimentation of Au NPs and RGO on a GCE electrode by electrochemical means. To begin, the GCE electrode was polished with an alumina-water slurry. After this, it was washed with water and ethanol. Then, 5 μL of the RGO dispersion (1 mg mL^{-1}) was put on the bare electrode. At room temperature (25 °C), the Au NPs deposited on the aforementioned RGO/GCE electrode by electrochemical means. The implementation of chronoamperometry was accomplished under the following conditions: the working electrode and the reference electrode were RGO/GCE and Ag/AgCl (3 M KCl), respectively, a platinum wire served as the auxiliary electrode, a 0.5 M H_2SO_4 solution comprising of 1% $HAuCl_4$ was used as the electrolyte and a voltage of -0.2 V was applied for 1 min.

2.3. Characterization

XRD patterns were obtained on a Bruker D8 Advance with Cu Kα radiation (λ = 0.1546 nm), and 2θ was measured in the range of 5° to 80°. For the Raman spectroscopy and optical analysis, a Raman microprobe (Renishaw RM1000) and UV-vis spectrophotometer (Perkin Elmer Lambda 950) were used, respectively. Fourier-transform infrared spectra (FTIR) were obtained with a Bruker Vertex 70 spectrometer.

2.4. Electrochemical determination

Throughout the experiments, a CHI430A electrochemical working station was used a three-electrode setup, which included RGO/Au/GCE as the working electrode, a Pt wire as the auxiliary electrode and Ag/AgCl as the reference electrode. Electrochemical impedance spectroscopy (EIS) is able to show the most evident characteristics of the resistance performance of the RGO/Au/GCE electrode. The set of experimental parameters were as follows: 0.1 M KCl as the electrolyte, 5 mV of amplitude, 5 mM $[Fe(CN)_6]^{3-/4-}$ as the probe, and 10^1-10^5 Hz as the frequency scope. With the purpose of determining ganopsoreric acid A, CV was implemented in 0.1 M PBS within a scan range of -1.5 to -0.7 V at a scan rate of 50 mV/s. With regards to DPV calculations, the scan range was -1.5 to -0.7 V with a scan rate of 0.6 mV/s, while the modulation took 0.05 s with an interval of 0.2 s.

2.5. Electrochemical determination of ganopsoreric acid A in ganoderma

The obtained vine fern herb was dried at a temperature of 60 °C for 4 hours, and after this, it was pulverized for use. Then, the pulverized power was refluxed in 70% aqueous ethanol (50 mL) at 80°C for 1 hour. A paper filter was used for filtration after the reflux cooled down completely. By mixing the extract and washings, approximately 40 mL of the obtained solution was dried under vacuum.

3. RESULTS AND DISCUSSION

Raman spectroscopy, which is highly sensitive towards variations of the electronic states of carbon-based materials, was used. It was found in the Raman spectra of RGO/Au and GO (as shown in Figure 1A) that the typical band at 1568 cm^{-1} is in accordance with graphite (G band, first-level scattering of E_{2g} phonons through sp^2 graphite atoms), while the other band at 1342 cm^{-1} corresponds to diamondoid (D band, breathing mode of κ-point photons of A_{1g} symmetry). In comparision with GO, RGO/Au nanocomposite possesses higher intensity ratio of D and G band (I_D/I_G), indicating that the average size of the sp^2 domains decreased and certain oxygen containing functional groups were removed as to RGO [25, 26].

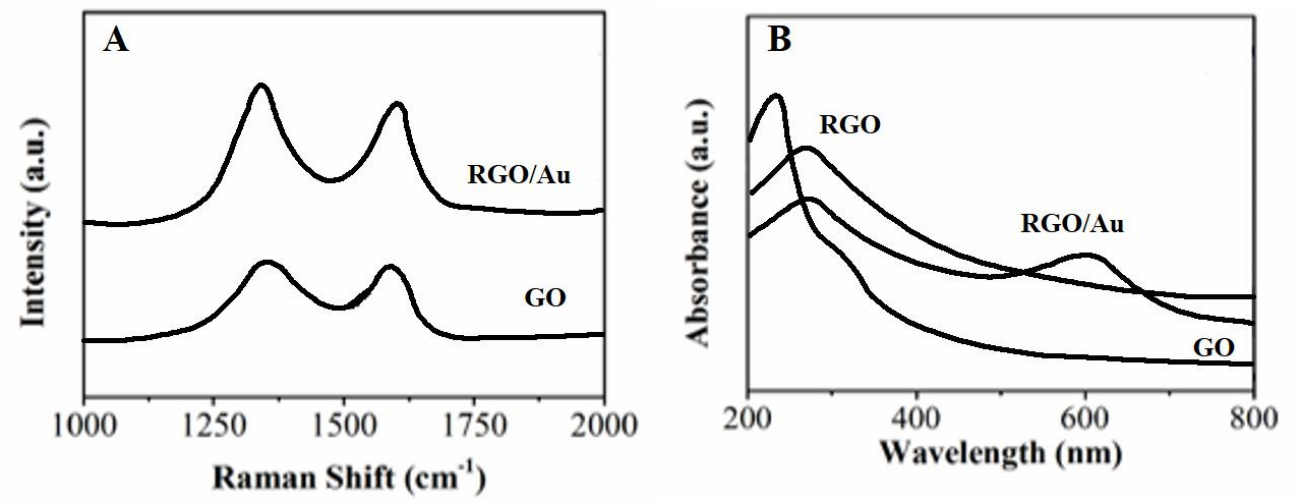

Figure 1. (A) Raman spectra and (B) UV-vis spectra of GO, RGO and the RGO/Au nanocomposite.

Figure 1B shows the UV-vis spectra of GO, RGO/Au and RGO. The absorption peak at 227 nm corresponds to the π—π* transition of the C-C bonds. In addition, the shoulder at 314 nm was caused by n—π* transitions of the C=O bonds. For the RGO spectrum, the absorption peak at 266 nm was likely contributed by a redshift of the peak of GO at 227 nm. As a result, not only was an appearance of a redshift observed, but also a disappearance of the shoulder absorption was observed, confirming that the reduction of GO to RGO was achieved successfully.Moreover, the absorption peak at 545 nm resulted from the surface plasmon absorption of Au NPs was observed in the spectrum of RGO/Au composite, suggesting that Au NPs was successfully electrodeposited on RGO [27].

Figure 2A shows the EDX characterization of the RGO/Au nanocomposite. In this figure, features of Au, C and O were seen, which is indicative of the high purity of the composite. Figure 2B shows the XRD patterns of the nanocomposite of GO, RGO and RGO/Au. For GO, a typical peak at 11.0° was observed, which was likely caused by the (001) crystal plane with *d*-spacing of 0.80 nm. For RGO, the peak at 2θ = 11.0° was not observed, revealing the success of the GO reduction. The peaks at 38.3°, 43.6°, 63.5° and 76.9° were in accordance with the crystal plane (111), (200), (220) and (311) of Au NPs. It is worth noting that the graphene oxide peak completely disappeared after the hydrothermal

reaction, suggesting the RGO has been formed in the composites. Furthermore, the week peak at 24.08° in RGO-Au composite illustrates the exfoliated RGO incorporated with Au NPs [28].

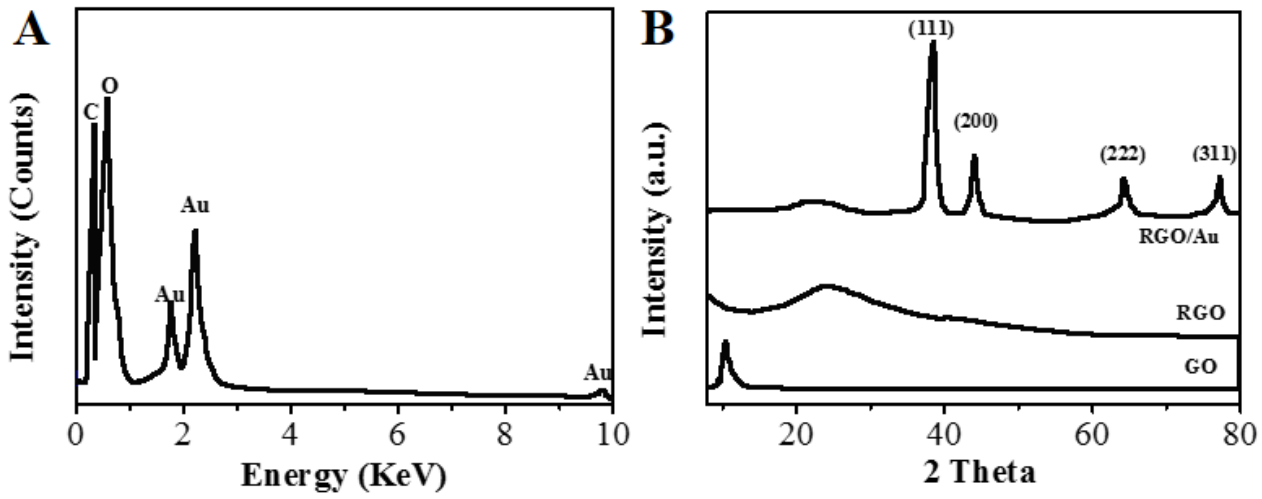

Figure 2. EDX spectrum of the RGO/Au composite, and (B) XRD patterns of GO, RGO and RGO/Au.

The determination of the effect of modification with RGO or RGO/Au on the electrochemical properties of GCE was realized using electrochemical impedance spectroscopy (EIS). In general, EIS comprises two features, namely, a semicircle resulting from the electron-transfer course and a straight line showing the diffusion course. In particular, through the calculation of the diameter of the semicircle, the electron-transfer resistance value can be determined. Non-Faradaic impedance biosensors perform impedance measurement in the absence of any redox probe. Bacteria detection is based on the impedance change upon the attachment of bacterial cells on an interdigitated microelectrode in the absence of any redox probe in the sample solution [29]. Figure 3 shows the EIS curves of clean GCE, the RGO/Au/GCE and RGO/GCE in 5 mM $[Fe(CN)_6]^{3-/4-}$ solution. In comparison with the vacant GCE electrode, the semicircular diameter acquired on the RGO/GCE electrode was larger, which indicates that charge transfer was obstructed when RGO was fixed to the GCE electrode. Oxygen groups that cover RGO can restrict the electron transfer of ferri/ferrocyanide, making the charge transfer more difficult [30]. However, the diameter of the semicircular acquired on the RGO/Au/GCE electrode did not catch up to that of the clean GCE electrode, showing a smaller electron-transfer resistance for the redox probe. As a result, by adding graphene sheets, the electrochemical performance of the electrode can be enhanced to a great extent.

Cyclic voltammograms (CVs) of ganopsoreric acid A (100 μM) in PBS were carried out on the different electrodes. Figure 4 shows that there was a mono-directional response with respect to the reduction of ganopsoreric acid A on all electrodes. Despite higher electron-transfer resistance being acquired on the RGO/GCE electrode, in comparison with the clean GCE, the reduction response of ganopsoreric acid A on the RGO/GCE electrode was clearly higher, which was contributed by the improved adsorption of ganopsoreric acid A molecules on the bigger BET surface area of RGO.

Moreover, on the RGO/Au/GCE electrode, the most obvious current response was observed with a favorable reduction potential of -1.06 V. Without the addition of ganopsoreric acid A, no peak was seen, indicating that the reduction peak was definitely ascribed to the reduction of ganopsoreric acid A.

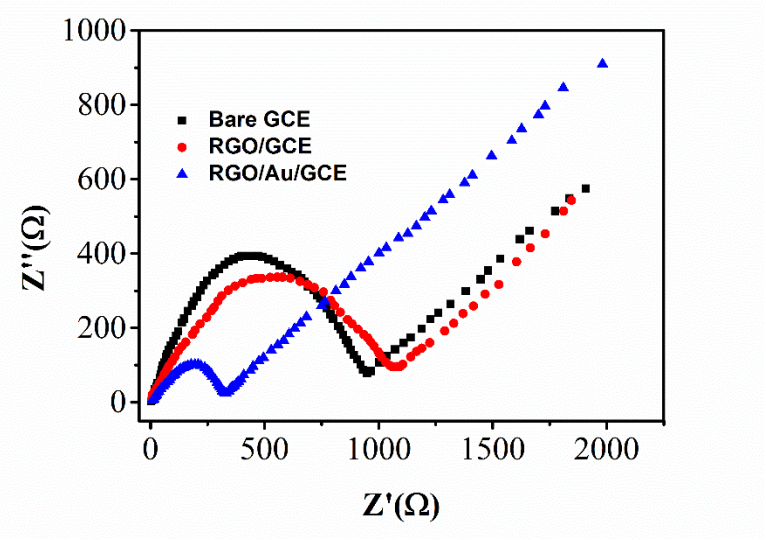

Figure 3. Nyquist diagrams acquired on clean GCE, the RGO/Au/GCE and the RGO/GCE electrodes.

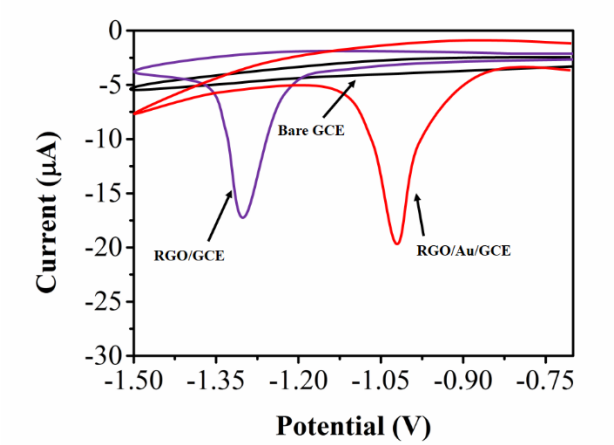

Figure 4. Cyclic voltammetry curves of 100 μM ganopsoreric acid A in PBS acquired on clean GCE, the RGO/GCE and the RGO/Au/GCE electrodes. Conditions: 0.2 M PBS, pH = 5.0, and scan rate = 50 mV/s.

This study analyzed the function of the electrolyte on the reduction of ganopsoreric acid A. Figure 5A illustrates the reduction values calculated in a variety of electrolytes, such as 0.1 M of PBS, $Na_2C_2O_4$, HAc-NaAc and H_2SO_4. It can be clearly seen that the highest reduction response of ganopsoreric acid A was acquired using PBS as the electrolyte. In consequence, PBS was adopted as the electrolyte solution in this research. In addition, this work investigated the effect of the pH of PBS on the reduction performance of ganopsoreric acid A, and the obtained results are demonstrated in

Figure 5B. It can be seen that the peak current increased when the pH value was increased from 3 to 5, and later, a decrease resulted when the pH value was further increased. As a result, when the pH value was equal to 5, the optimum value was gained, and therefore, this value was adopted in this work. Figure 5C shows that the electrodeposition time determines the relationship between the quantity of Au NPs and the current response. With a rise in electrodeposition time from 30 s to 60 s, the reduction current of ganopsoreric acid A was enhanced significantly. Upon a further increase of the deposition time to 90 s, a decrease of the current response was observed, as the electrochemical reaction was hindered on account of the polymerization of Au NPs.

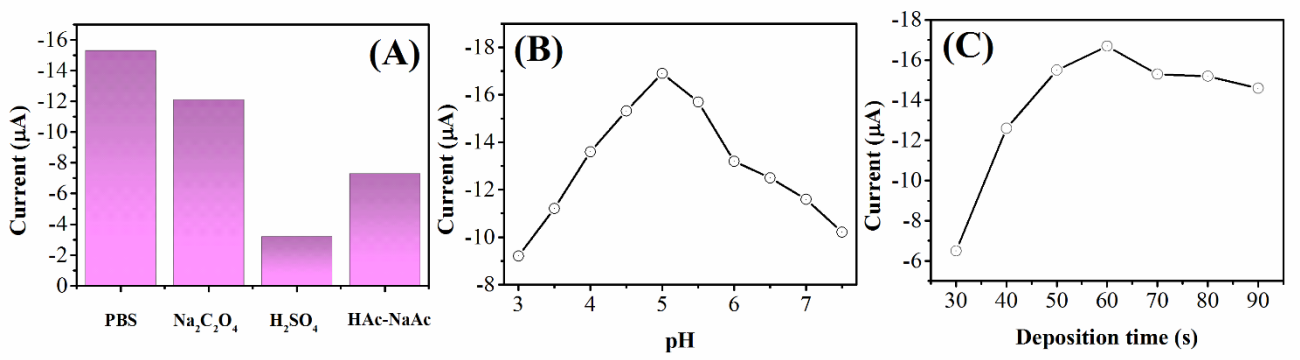

Figure 5. Influences of (A) electrolyte, (B) pH values of PBS and (C) electrodeposition time on ganopsoreric acid A reduction.

With the purpose of assessing the analytical performance of RGO/u/GCE under optimal conditions, differential pulse voltammetry (DPV) was used. On the RGO/Au/GCE electrode, DPV curves of ganopsoreric acid A at varying concentrations were obtained, as shown in Figure 6. There was a linear relationship between the current and the concentration of ganopsoreric acid A within the range of 2 to 600 μM, which was broader in comparison with an earlier report by Yang et al. [31], which reported that different kinds of the aflatoxins can be used for inhibiting the detection of ganopsoreric acid A. However, aflatoxins, such as avfA, omtA, and ver-1, which are used to code for key enzymes in aflatoxin biosynthesis, showed no electrochemical response at the detection potential. Therefore, the proposed method has the potential to detect ganopsoreric acid A in real conditions. The sensitivity of the proposed sensor was compared with that of other reported ganopsoreric acid A detection methods, and the results are presented in Table 1.

The assessment of the repeatability of the RGO/Au/GCE electrode was accomplished by the electrochemical reduction of 100 μM ganopsoreric acid A on ten clean RGO/Au/GCE electrodes. It was determined that the developed electrochemical sensor for the determination of ganopsoreric acid A had outstanding reproducibility with a measured relative standard deviation (RSD) of 3.15%. This study implemented five identical experiments to assess the stability of the RGO/Au/GCE electrode with respect to the electrochemical reduction of 100 μM ganopsoreric acid A. The current was reduced by 3.77%. On the RGO/Au/GCE electrode, the current response was nearly 96.4% of the original value after being stored in a freezer for 30 days, indicating the long-term storage stability of RGO/Au/GCE.

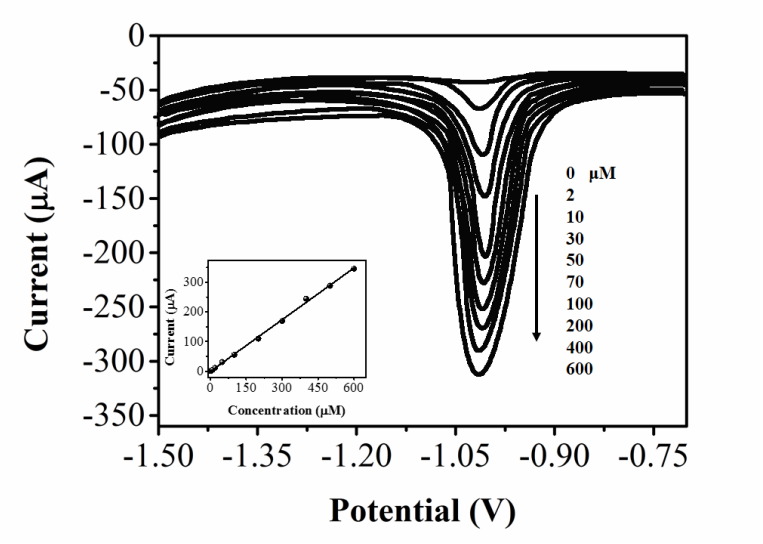

Figure 6. DPV curves of ganopsoreric acid A at a variety of concentrations acquired on the RGO/Au/GCE electrode. Inset: a plot of the reduction current as a function of ganopsoreric acid A concentration.

Table 1. Comparison of the present sensor with other ganopsoreric acid A detection methods.

Method	Linear range	Detection limit	Reference
HPLC	10 to 100μM	5μM	[32]
GC-MS	—	0.5 μM	[33]
RGO/Au/GCE	2 to 600 μM	1.5 μM	This work

Table 2. Detection of ganopsoreric acid A in four ganoderma extract specimens with RGO/Au/GCE electrode.

Sample	Addition (μM)	Found (μM)	Recovery (%)
1	0	17.27	—
	10	28.51	104.55
2	0	5.78	—
	50	56.21	100.77
3	0	8.96	—
	10	19.02	100.32
4	0	14.39	—
	50	64.11	99.57

The formed RGO/Au/GCE was adopted to determine ganopsoreric acid A in four grape fern herb extract specimens as well. With spike and recovery steps, the validation was calculated. Table 2 shows the acquired results. It can be seen from the obtained data that the sensor had outstanding performance with respect to the determination of ganopsoreric acid A in four extract specimens of grape fern herb, and the electrochemical sensor developed by us with the RGO/Au/GCE electrode had a high effectiveness in detecting ganopsoreric acid A in real herb specimens.

4. CONCLUSION

In conclusion, a facile chemical approach was adopted to modify a GCE electrode using RGO. Using electrodeposition, AuNPs were deposited on RGO. To develop an electrochemical sensor that can be used to determine ganopsoreric acid A, a RGO/Au/GCE electrode was adopted. The developed sensor showed a linear reaction within the scope of 2-600 μM. Moreover, excellent repeatability and good stability were established. This is the first time that a simple, dependable and sensitive electrochemical sensor has been developed to determine ganopsoreic acid A in extracts of a grape fern herb.

References

1. J. McAlpine, G. Hanley, M. Woo, A. Tone, N. Rozenberg, K. Swenerton, C. Gilks, S. Finlayson, D. Huntsman and D. Miller, *American Journal of Obstetrics and Gynecology*, 210 (2014) 471. e1.
2. S. Singh, A. Armstrong, J. Robke, S. Waggoner and R. Debernardo, *Gynecologic Oncology Case Reports*, 9 (2014) 24.
3. W. Wang, I. Kryczek, L. Tan, L. Zhao, G. He, L. Vatan, W. Szeliga, W. Zou and R. Liu, *The Journal of Immunology*, 194 (2015) 69.4.
4. S. Kar, J. Beesley, A. Al Olama, K. Michailidou, J. Tyrer, Z. Kote-Jarai, K. Lawrenson, S. Lindstrom, S. Ramus and D. Thompson, *Cancer Discovery*, 6 (2016) 1052.
5. C. Xintaropoulou, C. Ward, A. Wise, H. Marston, A. Turnbull and S.P. Langdon, *Oncotarget*, 6 (2015) 25677.
6. R. Massari, M. Barone, R. Basilico, C. Carella, A. Colasante, M. De Tursi, A. Filippone, L. Guetti and A. Mani, *Minerva Chirurgica*, 69 (2014) 17.
7. B. Erickson, J. Martin, M. Shah, J. Straughn and C. Leath, *Gynecologic Oncology*, 133 (2014) 142.
8. J. Loganathan, J. Jiang, A. Smith, A. Jedinak, A. Thyagarajan-Sahu, G. Sandusky, H. Nakshatri and D. Sliva, *International Journal of Oncology*, 44 (2014) 2009.
9. P. Twardowski, N. Kanaya, P. Frankel, T. Synold, C. Ruel, S. Pal, M. Junqueira, M. Prajapati, T. Moore and P. Tryon, *Cancer*, 121 (2015) 2942.
10. J. Kang, J. Jang, S. Mishra, H. Lee, C. Nho, D. Shin, M. Jin, M. Kim, C. Choi and S. Oh, *Journal of Ethnopharmacology*, 173 (2015) 303.
11. N. Santesso and L. Wieland, *European Journal of Integrative Medicine*, 8 (2016) 619.
12. E. Alonso, M. Ferronato, N. Gandini, M. Fermento, D. Obiol, A. López Romero, J. Arévalo, M. Villegas, M. Facchinetti and A. Curino, *Nutrition and Cancer*, 69 (2017) 29.
13. T. Ito, H. Urushima, M. Sakaue, S. Yukawa, H. Honda, K. Hirai, T. Igura, N. Hayashi, K. Maeda and T. Kitagawa, *Nutrition and Cancer*, 66 (2014) 377.
14. Y. Mizushina, N. Tanaka, A. Kitamura, K. Tamai, M. Ikeda, M. Takemura, F. Sugawara, A. Takao, A. Matsukage and S. Yoshida, *Biochemical Journal*, 330 (1998) 1325.
15. N. Tanaka, A. Kitamura, Y. Mizushina, F. Sugawara and K. Sakaguchi, *Journal of Natural Products*, 61 (1998) 193.
16. Y. Mizushina, I. Akira, O. Keisuke, F. SUGAWARA and K. Sakaguchi, *Biochemical Journal*, 350 (2000) 757.
17. Y. Mizushina, N. Takahashi, L. Hanashima, H. Koshino, Y. Esumi, J. Uzawa, F. Sugawara and K. Sakaguchi, *Bioorganic & Medicinal Chemistry*, 7 (1999) 2047.
18. F. Shahzad, S.A. Zaidi and C.M. Koo, *Sensors and Actuators B: Chemical*, 241 (2017) 716.
19. S. Ge, Y. Zhang, L. Zhang, L. Liang, H. Liu, M. Yan, J. Huang and J. Yu, *Sensors and Actuators B: Chemical*, 220 (2015) 665.
20. S. Azzouzi, H. Patra, M. Ali, M. Abbas, C. Dridi, A. Errachid and A. Turner, *Sensors and Actuators*

B: Chemical, 228 (2016) 335.
21. L. Qiu, L. Qiu, H. Zhou, Z. Wu, G. Shen and R. Yu, *New J Chem*, 38 (2014) 4711.
22. S. Radhakrishnan, K. Krishnamoorthy, C. Sekar, J. Wilson and S. Kim, *Appl. Ctatl. B-Environ.*, 148 (2014) 22.
23. M. Yola, T. Eren and N. Atar, *Sensors and Actuators B: Chemical*, 210 (2015) 149.
24. W. Liu, C. Li, Y. Gu, L. Tang, Z. Zhang and M. Yang, *Electroanalysis*, (2013) 2367.
25. X. Li, Q. Wang, Y. Zhao, W. Wu, J. Chen and H. Meng, *Journal of Colloid and Interface Science*, 411 (2013) 69.
26. S. Kamada, H. Nomoto, K. Fukuda, T. Fukawa, H. Shirai and M. Kimura, *Colloid Polym Sci*, 289 (2011) 925.
27. X. Lv and J. Weng, *Scientific Reports*, 3 (2013)
28. C. Xu, X. Wang and J. Zhu, *J. Phys. Chem. C.*, 112 (2008) 19841.
29. S. Radke and E. Alocilja, *Biosensors & Bioelectronics*, 20 (2005) 1662.
30. D. Jeykumari, S. Ramaprabhu and S. Narayanan, *Carbon*, 45 (2007) 1340.
31. Z. Yang, W. Shim, J. Kim, S. Park, S. Kang, B. Nam and D. Chung, *Journal of Food Protection®*, 67 (2004) 2622.
32. X. Wang, R. Dubois and D. Adams Jr, *Letters in Drug Design & Discovery*, 12 (2015) 140.
33. B. Ma, W. Ren, Y. Zhou, J. Ma, Y. Ruan and C.-N. Wen, *North American Journal of Medical Sciences*, 3 (2011) 495.